NANO LETTERS

Letter

pubs.acs.org/NanoLett

T Cell Activation is Determined by the Number of Presented Antigens

Janosch Deeg,[†,‡] Markus Axmann,[†,‡] Jovana Matic,[†,‡] Anastasia Liapis,[§] David Depoil,[§] Jehan Afrose,[§] Silvia Curado,[§] Michael L. Dustin,[§,∥] and Joachim P. Spatz*[,†,‡]

[†]Department of New Materials and Biosystems, Max Planck Institute for Intelligent Systems, Heisenbergstraße 3, D-70569 Stuttgart, Germany

[‡]Department of Biophysical Chemistry, University of Heidelberg, INF 253, D-69120 Heidelberg, Germany

[§]Skirball Institute of Biomolecular Medicine and Department of Pathology, New York University School of Medicine, New York, New York 10016, United States

[∥]Kennedy Institute of Rheumatology, Nuffield Department of Orthopedics, Rheumatology and Musculoskeletal Sciences, University of Oxford, Oxford, OX37FY, United Kingdom

S *Supporting Information*

ABSTRACT: Antigen recognition is a key event during T cell activation. Here, we introduce nanopatterned antigen arrays that mimic the antigen presenting cell surface during T cell activation. The assessment of activation related events revealed the requirement of a minimal density of 90−140 stimulating major histocompatibility complex class II proteins (pMHC) molecules per μm^2. We demonstrate that these substrates induce T cell responses in a pMHC dose-dependent manner and that the number of presented pMHCs dominates over local pMHC density.

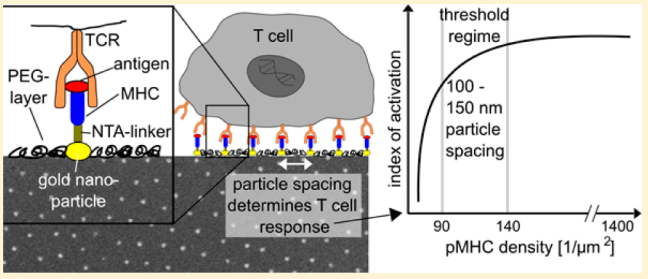

KEYWORDS: *Nanopattern, nanostructures, T cell activation, immunological synapse, artificial antigen-presenting cell, TCR microclusters*

A main task of the immune system is the recognition and elimination of pathogens. $CD4^+$ helper T cells are among the most prominent organizers in the adaptive phase of this multilayered defense system. In vivo, helper T cells constantly search for agonist peptides displayed by major histocompatibility class II proteins (pMHC) on the surface of antigen presenting cells (APCs) based on chemokine signals, confinement, and adhesion.[1] T cell receptor- (TCR) pMHC bonds and integrin-mediated adhesions between T cell and APC are initially organized in multiple small microclusters.[2−7] TCR microclusters translocate to the center of the contact area over time, thereby forming a temporary, highly structured cell−cell contact area termed immunological synapse (IS).[8,9] Signaling in microclusters is crucial and impacts the downstream outcomes of T cell activation including up-regulation of activation markers on the cell surface, cell proliferation, differentiation, and induction of cytokine secretion.[8]

A mature IS consists of well-defined ring-like structures with a micrometer scale bull's eye-like appearance. The innermost region of the IS is defined as the central supramolecular activation cluster (cSMAC) and is surrounded by the concentric peripheral supramolecular activation cluster (pSMAC).[10,11] While TCR microclusters are active signaling sites, the cSMAC can be subdivided into a signaling domain enriched in CD28 and protein kinase C-θ and a TCR-rich zone in which signaling becomes terminated.[12,13] The pSMAC plays a role in the stabilization of the IS structure through adhesion molecules—for example, integrin lymphocyte function antigen-1 (LFA-1) and its counterpart intercellular adhesion molecule-1 (ICAM-1)—allowing the passage of newly formed TCR microclusters toward the cSMAC.[10,14] However, this description portrays a "model" synapse. The IS is dynamic, and a variety of patterns and stages of receptor clustering have been observed.[8,15] For example, multifocal T cell-dendritic cell synapses lack the bull's eye patterning but have many similarities to the SMAC model.[16] Regardless, a stable IS contributes to efficient killing by cytotoxic T cells and is critical for formation of memory T cells.[17,18]

The appearance of TCR microclusters correlates with early activation events such as the elevation of the intracellular calcium (Ca^{2+}) level and polarization of the microtubule-organizing center (MTOC).[4,19] Microclusters are sites of recruitment of ZAP-70 and phosphorylated substrates including SH2 domains containing leukocyte protein SLP-76 and linker of activated T cells (LAT), that are central to TCR signaling.[4,20] These findings have led to the conclusion that microclusters,

Received: September 1, 2013
Revised: October 5, 2013
Published: October 11, 2013

   dx.doi.org/10.1021/nl403266t | *Nano Lett.* 2013, 13, 5619−5626

rather than larger features of the IS, are essential to signaling activity and seem to mediate both initial as well as sustained TCR signaling.[8,12,21] Despite the likely importance of pMHC preclustering and the stoichiometric arrangement of clusters previously documented on APCs,[22,23] the exact structural requirements for TCR triggering and how nanoscale events are translated into IS formation and T cell activation remain unclear.

T cells are highly sensitive to pMHC on the surface of APCs. It has been demonstrated that Ca^{2+} mobilization can be transiently mediated by contact of T cells with a single pMHC molecule on an APC and that full IS formation can be achieved with only 10 pMHC molecules.[24] Activation studies with soluble pMHC heterodimers, consisting of an agonist and an endogenous (self) peptide, proposed that the high sensitivity in vivo could be accomplished by formation of such pseudodimers. In this model the CD4 coreceptor forms a bridge between TCR-pMHC pairs, one pMHC being loaded with self-peptide.[25] Some support for this hypothesis was obtained using soluble dimers featuring distinct nanoscale spacers between the two MHC molecules, revealing an effect of receptor proximity. pMHC molecules linked through shorter cross-linkers showed higher potential to activate T cells.[26] However, soluble dimers lack the ability to transmit forces from the TCR that are thought to be critical for physiological T cell triggering and thus provide limited insight into events within the IS.[27,28]

Artificial APCs have been commonly used to study the impact of pMHC organization on T cell response. For instance, fluid-supported planar bilayers presenting mobile ligands have been applied to mimic the membrane conditions of an APC surface.[29] These have considerably contributed to the understanding of the molecular IS organization but are restricted in their control over molecular densities. To overcome this limitation and control diffusion of mobile pMHC molecules, lipid bilayers have been combined with electron beam lithography.[30] This approach established that 1−4 agonist pMHC molecules can trigger TCR signaling in the absence of endogenous pMHC.[12,31,32] Comparably, lithographic methods of patterning activation sites consisting of anti-CD3 surrounded by adhesive ICAM-1 on solid substrates can provide control of micrometer-scale IS organization.[33] A similar approach, which, in addition, included the use of anti-CD28 at the activating sites, established that T cells are sensitive to the micrometer-scale arrangement of costimulatory signals.[34] However, such lithographic methods also failed to provide insight into the nanoscale organization of the molecules involved.

Nanopatterned biointerfaces can be used for a precise control of both number and nanoscaled spatial arrangement of APC surface molecules. Such artificial cell presentation platforms allow for the site-specific directed immobilization of proteins at the molecular length scale,[35] and recently, even three-dimensional nanostructured water-in-oil droplets for homing T cells were reported.[36] Furthermore, these systems are scalable and sufficiently stable for clinical applications, such as controlled stimulation and expansion of T cells ex vivo.[37]

In the system that we present, proteins of interest are immobilized directly on nanoscaled gold (Au) particles, which are arranged in hexagonal patterns on glass coverslips. The particle size is such that in average either one or two proteins are selectively bound per Au particle (for details see SI). The particle spacing, that is, the lateral distance between two adjacent Au particles, can be varied from 15 to 300 nm.[38] This strategy prevents ligand mobility and allows for regulation of the number and nanoscale distribution of proteins that impact TCR triggering and other aspects of T cell activation. For stimulation experiments we used the well-characterized antigen-specific AND-TCR transgenic system in mouse $CD4^+$ T cells[39] (see SI for further details) and primarily focused on regulating the number and nanoscale arrangement of MHC-II molecules loaded with the specific peptide. We monitored both early and late responses by assessing cell spreading, MTOC polarization and cytokine secretion of T cells in contact with the nanopatterned substrates. We demonstrate here that T cells require a certain density of continuously nanopatterned pMHC molecules for spreading to occur. Only when this pMHC density threshold was met did T cells adhere to nanopatterned substrates, exhibiting MTOC polarization and interleukin-2 (IL-2) secretion. However, when cells were confronted with the same density of pMHC but arranged within confined and spatially separated micrometer scaled domains, they failed to attach and to secrete IL-2. T cell responses were restored; then the density of pMHC in the microstructures was increased to present a similar overall amount of pMHC as presented by an effective continuous nanopattern. These results strongly suggest the existence of a global pMHC density threshold, below which the initial steps of T cell activation do not occur.

Substrates were biofunctionalized with pMHC molecules following a spatial arrangement, local density, and orientation that are presumed to have a major impact on T cell activation. To this end, we applied block-copolymer micelle nanolithography (BCML) to fabricate surfaces patterned with arrays of quasi-hexagonally arranged Au nanoparticles. BCML is based on the self-assembly of polymeric micelles around Au cores. The Au-loaded micelles are deposited on solid substrates via dip- or spincoating. In a second step, the polymer shell is removed using oxygen plasma to produce an extensive centimeter-scaled nanopatterned array of Au-nanoparticles on a support surface (see Figure 1a, SI and Figure S1a and b).[35,40] We generated patterns with interparticle distances ranging from 30 to 300 nm by using diblock copolymers of different molecular weight. The resulting Au nanoparticles serve as anchor points for the site-specific attachment of linker molecules to which the proteins of interest can be conjugated. For this purpose we chose linker reagents that contain nitrilotriacetic acid−nickel (NTA−Ni) complexes and thiol functionalities. NTA−Ni^{2+} serves as anchor for any protein with a terminal poly histidine (His) tag.[41,42] To biofunctionalize the glass support surface, the space between the Au nanoparticles was filled with a poly ethylene glycol (PEG) layer (PEG couples covalently to glass through a silane group) prior to protein binding to reduce unspecific protein and cell substrate interaction to a minimum.[43] In addition to the highly regular nanopattern of Au particles, we generated a micropattern consisting of nanopatterned domains surrounded by nonadhesive (unpatterned) areas (Figure 1b). A two-step process that included BCLM followed by photolithography was used to fabricate these micronanopatterned substrates (see Figure S1c).[41]

We successfully demonstrated the site-specificity of protein attachment to the Au nanoparticles by immobilizing pMHC fluorescently labeled with [moth cytochrome C 88-103 (MCC)−Alexa Fluor 568/Atto 655]-IE^k-2xHis_6. Micronanopatterned substrates with attached fluorescent pMHC were visualized using fluorescence microscopy and showed a regular pattern of large bright polka dots (consisting of very small fluorescent spots), surrounded by a dark background,

dx.doi.org/10.1021/nl403266t | Nano Lett. 2013, 13, 5619−5626

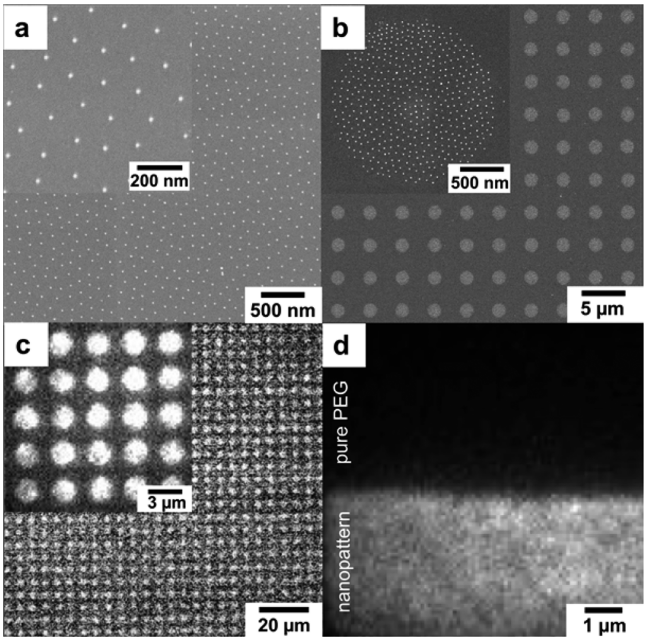

Figure 1. Scanning electron microscopy image of (a) an extensive continuous Au nanopattern and (b) a micronanopattern; (c) fluorescent microscopy image of pMHC labeled with a fluorescent Atto-655 dye and specifically immobilized on a micronanopattern; (d) fluorescent microscopy image of the border between a functionalized Au-patterned and a nonpatterned area; fluorescently labeled pMHC only binds to the area with embedded Au particles (bottom bright side).

consisting of PEG, with practically no proteins bound to it (see Figure 1c). Although the resolution of conventional fluorescence microscopy is limited to the visualization of the photolithographic microstructure and therefore does not allow for the discernment of the underlying nanopattern, specific binding to Au particles was observed and served as a functional assay.

Bulk measurements of fluorescently labeled pMHC allowed for the calculation of the average protein/particle ratio, which was found to be 1.6 ± 0.4 molecules per particle (for details see SI and Figure S2).

To assess the sensitivity of effector cells to the generated antigen arrays, both early and late T cell activation events were monitored. We focused our investigation on the following three phases of T cell response: (i) cell spreading, (ii) MTOC polarization, and (iii) IL-2 secretion. With this set of read-out parameters we were able to assess the ability of nanopatterns to function as APC surrogates and to investigate the effect of local and global pMHC distribution on different stages of T cell activation.

To assess T cell spreading, primary mouse $CD4^+$ T cell blasts were allowed to settle for 45 min on the pMHC-functionalized nanopatterned antigen arrays. This time point was chosen based on our experimental observations that the highest fraction of T cells was adherent at 15−90 min (see SI for further details) and based on previous studies which report T cell-APC adhesion to occur shortly after antigen detection and persisting up to several hours.[44] Hence, data acquisition at 45 min guarantees a high probability for generation of reproducible results. Reflection interference contrast microscopy (RICM) images (Figure 2a and b) show adherent cells as extended dark patches next to nonadherent cells (bright patches). Figure 2b shows T cells in contact with a nanopatterned and unpatterned part of the substrate. The unpatterned part of the surface (left side) lacks Au particles, and subsequently pMHC molecules, thus not allowing T cells to spread, whereas the nanopatterned part of the surface (right side) with Au particles and biofunctionalized with pMHC allows cells to adhere. Figure 2b shows that T cells selectively adhere to the pMHC-functionalized nanostructured area and that nonstructured areas are sufficiently passivated so that cells are unable to induce spreading and adhesion. MTOC polarization was accessed by immunofluorescence labeling and confocal imaging of α-tubulin near the center of the T cell-substrate interface and served as a visual marker for early T cell activation. As shown in Figure 2c, T cells seeded on a nanopatterned substrate were able to polarize, indicating an early stimulation of the T cell. We found that cell spreading and MTOC polarization were induced in T cells cultured on pMHC-functionalized nanopatterned surfaces featuring distances up to 150 nm, similarly to what was observed using glass surfaces entirely coated with pMHC (positive control). In contrast, the use of pure glass surfaces or passivated PEG surfaces, both lacking pMHC, did not result in early activation related events; see Table 1. This indicates that the presence of pMHC alone is sufficient for initiating adhesion and spreading of T cells using the system described in this study.

To quantify the effect of the pMHC particle spacing on T cell spreading, we measured the contact area of cells that were seeded and spread on different surfaces (see Figure 3a, light

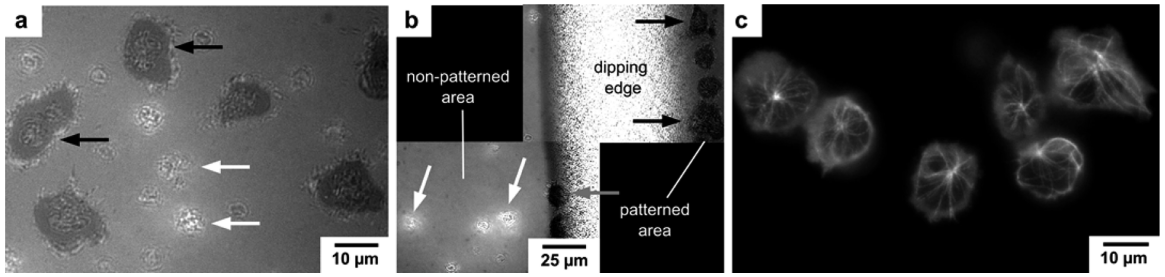

Figure 2. T cells on pMHC-presenting nanopatterned surfaces (spacing: 64 ± 9 nm) 45 min after seeding: (a) RICM image of adherent (dark, black arrows) and nonadherent (bright, white arrows) T cells; (b) nonadherent T cells on an unpatterned area (left) and adherent T cells on a nanopatterned and pMHC-functionalized area (right). The two regions are divided by the dipping edge—where an uncontrolled assembly of nanoparticles is common—a characteristic of the fabrication process. The gray arrow indicates a cell adhering to the dipping edge. Note: Figure 2b consists of two separate images since, due to the high magnification (63×), it was not possible to capture both sides of the dipping edge within one image. (c) Fluorescent image of polarized α-tubulin in T cells seeded on a nanopatterned surface.

dx.doi.org/10.1021/nl403266t | *Nano Lett.* 2013, 13, 5619−5626

Table 1. Successful (checkmarks) and Unsuccessful (×'s) Adhesion and Centrosome Polarization on Different Surfaces[a]

	glass pMHC	nano pMHC	glass	PEG
spreading	✓	✓	×	×
polarization	✓	✓	×	×

[a]Glass = random coating; nano = nanopattern.

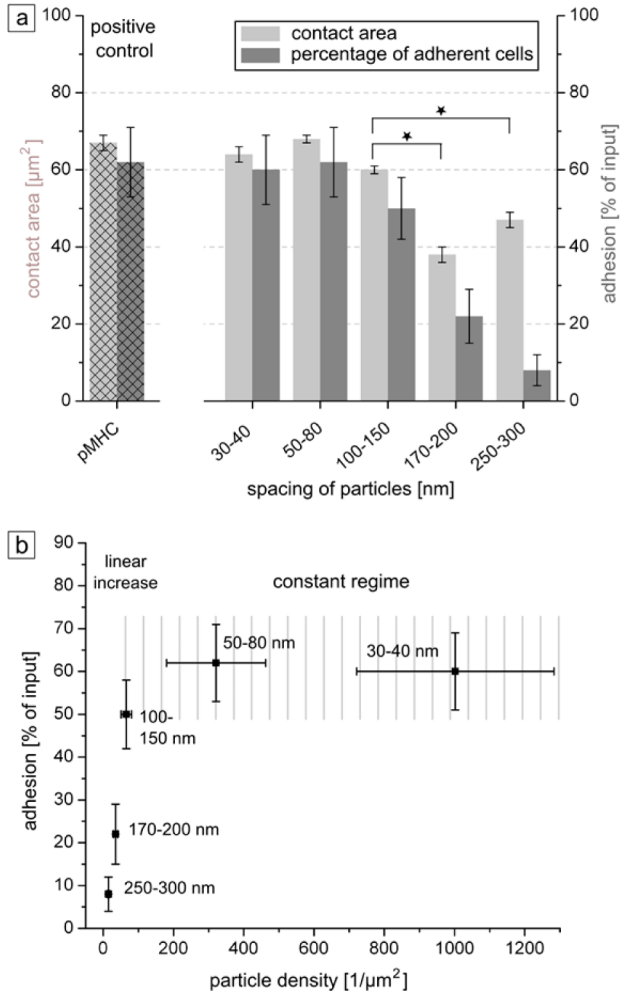

Figure 3. (a) Mean cell contact area (light gray bars) and percentage of adherent T cells (dark gray bars) after (45 ± 15) min of cell–substrate contact. Nanopatterns featuring different interparticle spacings and a positive control, which was a glass surface entirely coated with pMHC, were also included. Spreading was not observed on negative control (PEG) surfaces. Stars in part a indicate very significant differences of mean values according to Welch's *t*-test: $*p < 0.0001$; $n > 100$ spread cells for each mean value, except for cells on surfaces with particle distances greater than 150 nm (due to very low cell adhesion numbers). (b) Percentage of adherent cells (data presented as in a) plotted as a function of particle density. In both graphs (a and b) *y*-error bars correspond to the standard error of the mean, *x*-error bars in b correspond to the error of the single value (also see error discussion in the SI).

gray bars) as well as the percentage of adherent cells in relation to the overall cell input (see Figure 3a, dark gray bars). A significant decrease in the average contact area was observed for T cells seeded on substrates with distances greater than 150 nm between the protein anchorage points. Even more significant was the decrease of the number of cells that spread. We found that most cells failed to adhere on nanopatterned surfaces with spacing greater than 150 nm (see Figure 3a, dark gray bars). The percentage of adherent T cells was highest (approximately 60%) on nanopatterned surfaces featuring a shorter interparticle distance (30–80 nm). The number of adherent cells continuously decreased, down to only 10% of T cells cultured on surfaces featuring particle spacing of 250–300 nm (see also error discussion in SI). Plotting adhesion versus particle density further emphasizes the rapid quasi-linear increase in percentage of adhesion as densities approach 100 particles per μm (Figure 3b). Saturation of cell adhesion was observed for higher particle densities. These data indicate the requirement of a minimal density of pMHC molecules for initiation of T cell adhesion and spreading.

To assess whether the nanopatterned substrates supported T cell activation long-term, we monitored the amount of IL-2 secreted by T cells activated on these substrates 24 h after the cells were seeded. In Figure 4a the *index of activation*, $I_{activation}$, is shown as a function of the particle spacing. $I_{activation}$ corresponds to the amount of IL-2 (X_{IL2}) secreted by approximately 1.5×10^5 cells 24 ± 1 h after cells were seeded on the individual surfaces related to the amount of IL-2 ($X_{control}$) secreted by the same number of cells on positive control surfaces entirely coated with pMHC during the same experimental time: $I_{activation} = X_{IL2}/X_{control}$. Surfaces entirely covered with bioinert PEG layer, which is known to prevent any cellular interaction, were used a negative control ("PEG"). A second positive control ("0" spacing) consisted of a surface fully covered with Au and functionalized with pMHC, similar to substrates routinely used for T cell activation. No significant difference was observed in IL-2 secretion of cells seeded on adsorption-based pMHC-coated glass surfaces versus cells on Au-coated surfaces functionalized with NTA-Ni^{2+}-pMHC (see Figure 4a). We therefore conclude that, at high pMHC densities, the immobilization strategy does not impact IL-2 secretion. As expected, the highest values of $I_{activation}$ were obtained for cells seeded on pMHC surfaces (positive control), whereas the lowest values were observed for cells on PEG surfaces (negative control). Figure 4b shows only the mean values for $I_{activation}$ obtained on nanopatterns as a function of particle spacing. T cells seeded on nanostructures showed a quasi-linear decrease of IL-2 secretion with increasing particle distance. However, as represented in Figure 4c, which shows the $I_{activation}$ plotted as a function of particles per μm^2, we observed a collapse of IL-2 secretion under conditions of particle density below, and a constant IL-2 secretion above this threshold particle density of approximately 100 particles per μm^2. At a particle density below 100 particles per μm^2 IL-2 secretion was shown to depend linearly on the particle density. Figure 4d shows a selective enlargement of this quasi-linear section of the plot in Figure 4c (for further discussion see below).

Importantly, the response of the T cells to the continuous nanopatterned pMHC could reflect either the requirement for a certain number of pMHC molecules in the contact area or a critical distance between pMHC molecules. To further test these hypotheses, we compared the effect of local versus global particle density on T cell response. Continuous nanoparticle

dx.doi.org/10.1021/nl403266t | *Nano Lett.* 2013, 13, 5619–5626

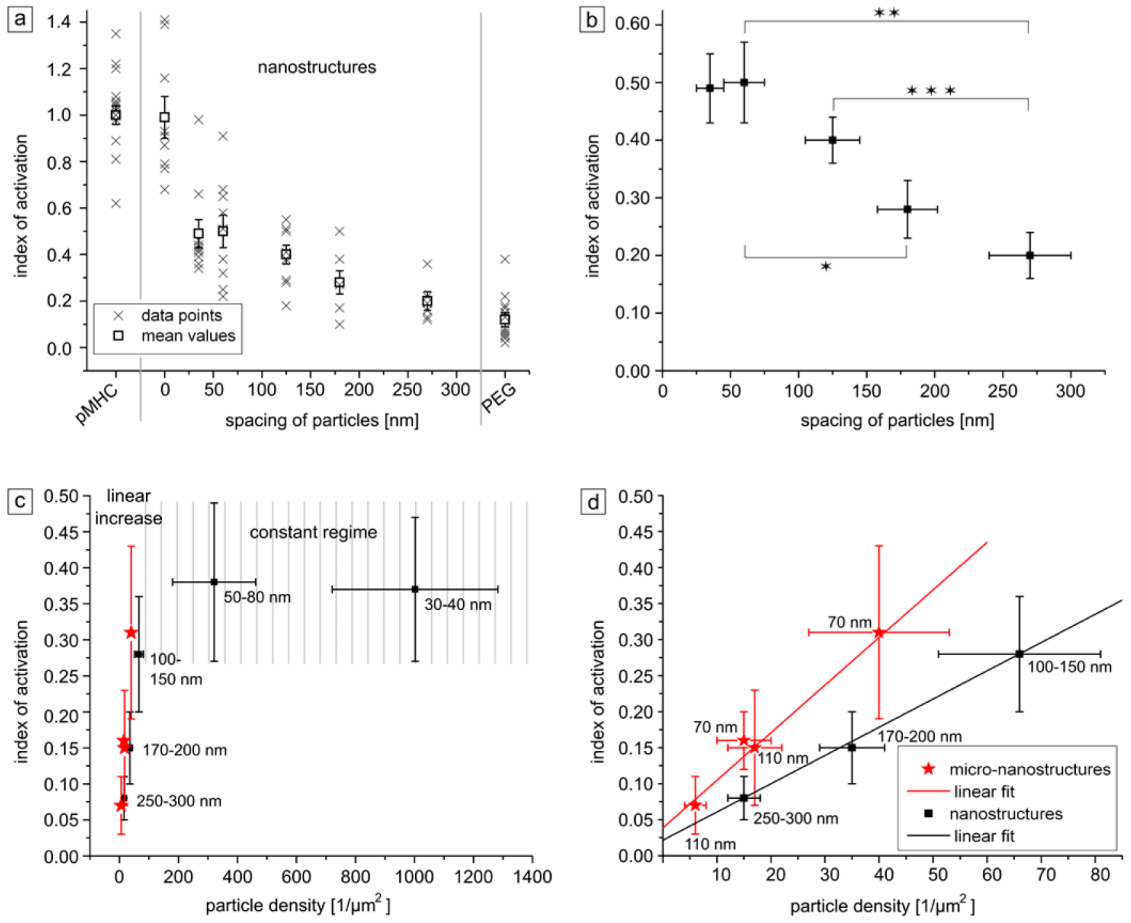

Figure 4. Index of activation (IL-2 secretion) of T cells seeded on different surfaces plotted against the distance between pMHC-ligands (a and b) or global particle density (c and d). (a) Individual measurements and mean values of the activation rate ($I_{activation}$) as a function of particle spacing. Data obtained using cells seeded on PEG-coated surfaces (negative control, processed identically with the same linker and protein solutions as for the nanopatterned surfaces) is presented on the right side of the graph, whereas data for cells seeded on continuously pMHC-coated surfaces (positive control) are shown on the left side of the graph. Substrates with "0" particle distance (second positive control) were produced using surfaces entirely coated with Au. (b) Representation of mean values only, obtained using the different nanopatterned surfaces (also represented in a). Stars in b indicate significant differences of mean values according to Welch's *t*-test: $*p = 0.045$; $**p = 0.012$; $***p = 0.005$. (c) Mean values of the index of activation of cells cultured on nanopatterned (black data points, see a) and micronanopatterned (red data points, $n = 4$ for each data point) as a function of global particle density. (d) Selective enlargement of the linear section of plot (c). For each data point in c and d the amount of IL-2 secreted by T cells on the negative control surfaces was set as the background value and subtracted from the IL-2 values measured for each nanopatterned substrate. The *y*-error bars in all graphs correspond to the standard error of the mean, *x*-error bars to the standard deviation of the single value. In (c) and (d) Gaussian error propagation was additionally applied to determine deviations of particle densities and background-corrected index of activation (see also error discussion in SI).

arrays, as shown in Figure 1a, have identical local and global particle densities. In contrast, micronanopatterned particles, as shown in Figure 1b, can be prepared with the same local density, but lower global densities. Conversely, micronanopatterned surfaces with the same global particle density as continuous nanopatterned surfaces feature much more densely arranged particles within their microdomains (see Table 2).

We prepared four micronanopatterned surfaces with a global particle density between 7 and 46 particles per μm^2. The local particle density values (within the microdomains) were chosen based on particle density values that cause spreading, MTOC polarization, and IL-2 secretion on continuous nanopatterned surfaces. However, the global particle density of micro-nanopatterned surfaces was in the range where adhesion and spreading on continuous nanopatterned pMHC was reduced or prevented (see Table 2). Using this strategy we were able to discern whether spatially confined activating islands are sufficient to induce T cell adhesion, spreading, and IL-2

Table 2. Features of Micronanopatterns

Dimensions of Micronanopatterns				
diameter of microdomains (D, μm)	$D = 1.5$	$D = 1.5$	$D = 1.5$	$D = 1.5$
microdomain grid spacing (d, μm)	$d = 3$	$d = 5$	$d = 3$	$d = 5$
interparticle distance (nm)	70 ± 10	70 ± 10	110 ± 15	110 ± 15
local particle density in microdomain (particles/μm^2)	236 ± 67	236 ± 67	95 ± 26	95 ± 26
global particle density (particles/μm^2)	46 ± 15	17 ± 5	19 ± 6	7 ± 2
particle spacing of extended nanopattern with the respective global particle density (nm)	158	261	247	406

dx.doi.org/10.1021/nl403266t | *Nano Lett.* 2013, 13, 5619−5626

production or whether the overall availability of pMHC is the critical parameter for T cell stimulation.

T cells seeded on micronanopatterned substrates showed less adhesion (10−18%) and MTOC polarization than cells seeded on extended nanopatterns exhibiting a similar spacing between particles as the micronanopatterns. Accordingly, IL-2 secretion of cells seeded on micronanopatterns was very low (see red stars in Figure 4c and enlargement in Figure 4d). Secreted IL-2 levels were in the range of those of cells cultured on surfaces with extended patterns with a much less dense nanopattern (larger spacing) but identical global particle density. Nevertheless, a slight increase of IL-2 secretion was observed when using micronanopatterned substrates as compared with extended nanopattern substrates (see Figure 4d). Therefore, our data suggest that activation of T cells is predominantly regulated by the global pMHC concentration and depends on the local spacing of the pMHC pattern only as a higher order effect. A possible explanation for this finding could be that IS formation is critically dependent on cell spreading. Above the particle spacing threshold of approximately 150 nm it becomes unlikely that T cells encounter sufficient anchor points to initiate microcluster formation spreading, and thus, subsequent signaling that would result in a productive T cell response fails. Since the proximity of pMHC molecules supports microcluster formation,[26] we assume that particle spacing also plays a key role. However, in our system such a distance effect of pMHC molecules is only detectable as a secondary effect. For T cell activation by an artificial APC system lacking any additional adhesive ligands the essential requirement seems to be that microcluster formation is not restricted to certain areas but can occur over the entire cell-artificial APC contact area. Only in such cases T cells can successfully spread and adhere. Nevertheless, we observe slightly increased $I_{activation}$ values within the linear transition regime for cells seeded on micronanopatterns and assume that this effect is due to ligand proximity. Probably, although the global particle density on micronanopatterns is very low, cells are able to form microclusters within the microdomains, however in most cases not in a sufficient extent to initiate adhesion. In contrast, on extensive nanopatterns, featuring global particle densities in the same regime, TCR assembly fully fails due to the high spacing/low density of pMHC molecules. We speculate that the quasi-proportional increase of $I_{activation}$ with density of pMHC in the transition regime is due to an increasing probability of successful microcluster formation with subsequent adhesion and IL-2 secretion of an individual T cell. Averaged over a high cell number, the development of $I_{activation}$ results in such a linear behavior. However, at the same time, these data cannot exclude that each cell may act as a digital antigen counter system that needs to detect a certain number of pMHC molecules to initiate activation pathways.

We demonstrate that the biocompatible nanopatterned antigen arrays generated in this study can be used to modulate the degree of T cell activation by controlling the number and spatial arrangement of TCR ligands on the substrate. Once seeded on these substrates, following TCR triggering, T cells adhered, polarized the MTOC, and secreted IL-2. For cell spreading to be initiated, T cells require a minimum particle density of approximately 100 particles per μm^2, which corresponds to a particle spacing of approximately 115 nm. At greater particle distances (especially above 150 nm) spreading and IL-2 secretion are strongly reduced. As shown in Figures 3b and 4c, at particle density values up to approximately 100 particles per μm^2, both cell spreading and IL-2 secretion show a linear increase with increasing density (decreasing particle distance). At higher particle densities (distances below 150 nm), both cell spreading and IL-2 secretion levels reach a plateau. In our system the T cell activation effects we have shown seem to be predominantly regulated by the particle density and not the interparticle spacing. On nanopatterns of hexagonally arranged particles a particle distance of 150 nm is equivalent to a particle density of 70 per μm^2. Assuming an average particle occupation of 1.6 ± 0.4 (for details see SI), the pMHC density on these substrates corresponds to 112 ± 28 pMHC molecules per μm^2. Hence, the threshold for adhesion and IL-2 production is approximately at 90−140 molecules per μm^2, indicated by a collapse of the cell response when pMHC molecules are more scattered, and therefore, fewer molecules are available for cells to attach to.

By comparing local with global particle density of extended and micronanopattern surfaces, we found that events related to T cell activation such as spreading and IL-2 secretion are determined by the entire number of pMHCs available to the T cells, rather than the peak density in subregions corresponding in size to SMACs. The critical TCR ligand density found in this study is significantly higher than the previously reported low pMHC thresholds, some of which were determined to be in the one digit range.[24,32] However, in contrast to previous reports where T cell activation was achieved using real APCs or lipid bilayers presenting ICAM-1 together with pMHC, our purely pMHC-based approach did not provide costimulation or adhesive support. Nevertheless, the substrates used in the study were capable of stimulating effector T cells through sole exposure to pMHC. Provided that the global pMHC density is high enough, T cell blasts can adhere and produce IL-2 without the presence of additional adhesive or costimulatory molecules. We assume that pMHC/TCR microclusters are able, up to a certain extent, to take on the role of adhesive molecular bonds. In this case, however, a locally confined high pMHC density is insufficient for T cell adhesion, spreading and activation. Instead, T cells require a global pMHC density to overcome barriers for cell spreading. Once spreading is initiated, further signaling induces cytokine secretion. It has been previously observed that surfaces uniformly coated with anti-CD3 induce microclustering of TCR.[45] This clustering may facilitate adhesion and spreading in the absence of adhesion molecules. Prior studies on LFA-1 deficient mice suggest that LFA-1 increases the sensitivity of the T cell to antigen up to 100-fold.[46] Therefore, we speculate that adhesive molecules play an important role during the process of T cell activation only when the global pMHC density is below 112 ± 28 molecules per μm^2. Most probably, on substrates where pMHC molecules are more scattered than this threshold range, pMHCs are unable to compensate for the absence of adhesive molecules. We speculate that under such conditions the presence of adhesive ligands is pivotal and supports TCR clustering and signaling resulting in further activation events such as cytokine secretion. In contrast, on substrates with a sufficient pMHC density, additional costimulatory and adhesion-mediating molecules may function only as signal amplifier and may not be a crucial requirement. So far, several studies titrated pMHC and measured adhesion, but generally the density of pMHC was not reported.[47,48] Immobile pMHC in supported planar bilayers were shown to mediate adhesion of T cell hybridomas at 1000 molecules/μm^2, but not 50 molecules/μm^2,[49] which is

dx.doi.org/10.1021/nl403266t | Nano Lett. 2013, 13, 5619−5626

consistent with our current studies. Establishing the quantitative requirements for providing a TCR-only signal through nanopatterning may provide the possibility to generate substrates that could be used to induce antigen-specific T cell tolerance.[50] The determination of rupture forces between T cell-APC conjugates has already revealed that the development of adhesion forces correlates with the dynamics of IS formation.[51,52] Future studies could therefore further address the presence and development of adhesion forces between the T cell and the substrate to better understand the role of pMHC-TCR complexes in adhesion and spreading, since both are required for a successful activation of T cells.

In conclusion, to better investigate the complex process of T cell activation, we introduce an approach, already successfully applied in other biological studies,[53,54] to the field of immunology: nanopatterned substrates. By comparing local and global pMHC densities we showed that local pMHC clustering is not of predominant importance for T cell activation but does have an influence on higher order effects. Furthermore, a global pMHC density of approximately 112 ± 28 molecules per μm^2 was identified as a threshold for T cell activation when based only on pMHC.

■ ASSOCIATED CONTENT

Supporting Information

Materials and methods for all applied fabrication and experimental techniques and an error discussion. This material is available free of charge via the Internet at http://pubs.acs.org.

■ AUTHOR INFORMATION

Corresponding Author

*E-mail: spatz@is.mpg.de.

Author Contributions

J.D. performed the cell experiments. M.A. and J.D. performed the fluorescence microscopy experiments to determine particle occupation. D.D. and J.A. provided cells and proteins. J.D., J.P.S., J.M., A.L., S.C., D.D., and M.L.D. are responsible for the conceptual design of the experiments. S.C. was further responsible for the entire organization of the research project. The manuscript was written with contributions from all authors.

Notes

The authors declare no competing financial interest.

■ ACKNOWLEDGMENTS

Nina Grunze's corrections, editing, and revisions contributed a lot to the improvement of the manuscript and were warmly appreciated. We thank Dr. Timo Maier for setting-up and maintaining the reflection interference contrast microscope. M.A. acknowledges the Erwin Schrödinger Fellowship Program of the Austrian Science Fund (FWF): J3086-B11. The work was part of the European Union Seventh Framework Program (FP7/2007-2013) under grant agreement no. NMP4-LA-2009-229289 NanoII and by the National Institutes of Health through the NIH Roadmap for Medical Research (PN2 EY 016586). This work is also part of the excellence cluster CellNetwork at the University of Heidelberg. J.P.S. is the Weston Visiting Professor at the Weizmann Institute of Science. We acknowledge the support of the Max Planck Society and the Wellcome Trust.

■ REFERENCES

(1) Lämmermann, T.; Bader, B. L.; Monkley, S. J.; Worbs, T.; Wedlich-Söldner, R.; Hirsch, K.; Keller, M.; Förster, R.; Critchley, D. R.; Fässler, R.; Sixt, M. *Nature* **2008**, *453*, 51−5.

(2) Yokosuka, T.; Saito, T. *Immunol. Rev.* **2009**, *229*, 27−40.

(3) Kaizuka, Y.; Douglass, A. D.; Varma, R.; Dustin, M. L.; Vale, R. D. *Proc. Natl. Acad. Sci. U.S.A.* **2007**, *104*, 20296−20301.

(4) Campi, G.; Varma, R.; Dustin, M. L. *J. Exp. Med.* **2005**, *202*, 1031−6.

(5) Lillemeier, B. F.; Mörtelmaier, M. A.; Forstner, M. B.; Huppa, J. B.; Groves, J. T.; Davis, M. M. *Nat. Immunol.* **2010**, *11*, 543.

(6) Sherman, E.; Barr, V.; Manley, S.; Patterson, G.; Balagopalan, L.; Akpan, I.; Regan, C. K.; Merrill, R. K.; Sommers, C. L.; Lippincott-Schwartz, J.; Samelson, L. E. *Immunity* **2011**, *35*, 705−720.

(7) Mossman, K. D.; Campi, G.; Groves, J. T.; Dustin, M. L. *Science* **2005**, *310*, 1191−1193.

(8) Dustin, M. L.; Groves, J. T. *Annu. Rev. Biophys.* **2012**, *41*, 543−56.

(9) Fooksman, D. R.; Vardhana, S.; Vasiliver-Shamis, G.; Liese, J.; Blair, D. A.; Waite, J.; Sacristán, C.; Victora, G. D.; Zanin-Zhorov, A.; Dustin, M. L. *Annu. Rev. Immunol.* **2010**, *28*, 79−105.

(10) Grakoui, A.; Bromley, S. K.; Sumen, C.; Davis, M. M.; Shaw, A. S.; Allen, P. M.; Dustin, M. L. *Science* **1999**, 221.

(11) Monks, C.; Freiberg, B.; Kupfer, H.; Sciaky, N.; Kupfer, A. *Nature* **1998**, *395*, 82−86.

(12) Varma, R.; Campi, G.; Yokosuka, T.; Saito, T.; Dustin, M. L. *Immunity* **2006**, *25*, 117−27.

(13) Yokosuka, T.; Kobayashi, W.; Sakata-Sogawa, K.; Takamatsu, M.; Hashimoto-Tane, A.; Dustin, M. L.; Tokunaga, M.; Saito, T. *Immunity* **2008**, *29*, 589−601.

(14) Groves, J. T. *Curr. Opin. Chem. Biol.* **2006**, *10*, 544−50.

(15) Irvine, D. J.; Doh, J. *Sem. Immunol.* **2007**, *19*, 245−54.

(16) Tseng, S.-Y.; Waite, J. C.; Liu, M.; Vardhana, S.; Dustin, M. L. *J. Immunol.* **2008**, *181*, 4852−4863.

(17) Stinchcombe, J. C.; Bossi, G.; Booth, S.; Griffiths, G. M. *Immunity* **2001**, *15*, 751−761.

(18) Scholer, A.; Hugues, S.; Boissonnas, A.; Fetler, L.; Amigorena, S. *Immunity* **2008**, *28*, 258−270.

(19) Hashimoto-Tane, A.; Yokosuka, T.; Sakata-Sogawa, K.; Sakuma, M.; Ishihara, C.; Tokunaga, M.; Saito, T. *Immunity* **2011**, *34*, 919−31.

(20) Yokosuka, T.; Sakata-Sogawa, K.; Kobayashi, W.; Hiroshima, M.; Hashimoto-Tane, A.; Tokunaga, M.; Dustin, M. L.; Saito, T. *Nat. Immunol.* **2005**, *6*, 1253−1262.

(21) Yokosuka, T.; Saito, T. *Curr. Top. Microbiol. Immunol.* **2010**, *340*, 81−107.

(22) Kropshofer, H.; Spindeldreher, S.; Röhn, T. A.; Platania, N.; Grygar, C.; Daniel, N.; Wölpl, A.; Langen, H.; Horejsi, V.; Vogt, A. B. *Nat. Immunol.* **2002**, *3*, 61−68.

(23) Fooksman, D. R.; Grönvall, G. K.; Tang, Q.; Edidin, M. *J. Immunol.* **2006**, *176*, 6673−6680.

(24) Irvine, D. J.; Purbhoo, M. A.; Krogsgaard, M.; Davis, M. M. *Nature* **2002**, *419*, 845−9.

(25) Krogsgaard, M.; Li, Q.-J.; Sumen, C.; Huppa, J. B.; Huse, M.; Davis, M. M. *Nature* **2005**, *434*, 238−43.

(26) Cochran, J. R.; Cameron, T. O.; Stone, J. D.; Lubetsky, J. B.; Stern, L. J. *J. Biol. Chem.* **2001**, *276*, 28068−28074.

(27) Kim, S. T.; Takeuchi, K.; Sun, Z.-Y. J.; Touma, M.; Castro, C. E.; Fahmy, A.; Lang, M. J.; Wagner, G.; Reinherz, E. L. *J. Biol. Chem.* **2009**, *284*, 31028−37.

(28) Li, Y.-C.; Chen, B.-M.; Wu, P.-C.; Cheng, T.-L.; Kao, L.-S.; Tao, M.-H.; Lieber, A.; Roffler, S. R. *J. Immunol.* **2010**, *184*, 5959−63.

(29) Dustin, M. L. *Curr. Top. Microbiol. Immunol.* **2010**, *340*, 1−24.

(30) Mossman, K. D.; Campi, G.; Groves, J. T.; Dustin, M. L. *Science (New York, N.Y.)* **2005**, *310*, 1191−3.

(31) Ma, Z.; Sharp, K. A.; Janmey, P. A.; Finkel, T. H. *PLoS Biol.* **2008**, *6*, e43.

(32) Manz, B. N.; Jackson, B. L.; Petit, R. S.; Dustin, M. L.; Groves, J. *Proc. Natl. Acad. Sci. U.S.A.* **2011**, *108*, 9089−94.

(33) Doh, J.; Irvine, D. J. *Proc. Natl. Acad. Sci. U.S.A.* **2006**, *103*, 5700−5.

(34) Shen, K.; Thomas, V. K.; Dustin, M. L.; Kam, L. C. *Proc. Natl. Acad. Sci. U.S.A.* **2008**, *105*, 7791−7796.
(35) Lohmüller, T.; Aydin, D.; Schwieder, M.; Morhard, C.; Louban, I.; Pacholski, C.; Spatz, J. P. *Biointerphases* **2011**, *6*, MR1.
(36) Platzman, I.; Janiesch, J.-W.; Spatz, J. P. *J. Am. Chem. Soc.* **2013**, *135*, 3339−42.
(37) Porter, D. L.; Levine, B. L.; Kalos, M.; Bagg, A.; June, C. H. *N. Engl. J. Med.* **2011**, *365*, 725−733.
(38) Glass, R.; M ller, M.; Spatz, J. P. *Nanotechnology* **2003**, *14*, 1153−1160.
(39) Kaye, J.; Vasquez, N. J.; Hedrick, S. M. *J. Immunol.* **1992**, *148*, 3342−3353.
(40) Spatz, J. P.; Mössmer, S.; Hartmann, C.; Möller, M.; Herzog, T.; Krieger, M.; Boyen, H.-G.; Ziemann, P.; Kabius, B. *Langmuir* **2000**, *16*, 407−415.
(41) Aydin, D.; Schwieder, M.; Louban, I.; Knoppe, S.; Ulmer, J.; Haas, T. L.; Walczak, H.; Spatz, J. P. *Small* **2009**, *5*, 1014−1018.
(42) Wegner, S. V.; Spatz, J. P. *Angew. Chem., Int. Engl.* **2013**, *52*, 7593−7596.
(43) Blümmel, J.; Perschmann, N.; Aydin, D.; Drinjakovic, J.; Surrey, T.; Lopez-Garcia, M.; Kessler, H.; Spatz, J. P. *Biomaterials* **2007**, *28*, 4739−47.
(44) Kumari, S.; Vardhana, S.; Cammer, M.; Curado, S.; Santos, L.; Sheetz, M. P.; Dustin, M. L. *Front. Immunol.* **2012**, *3*, 230.
(45) Bunnell, S. C. *J. Cell Biol.* **2002**, *158*, 1263−1275.
(46) Bachmann, M. F.; McKall-Faienza, K.; Schmits, R.; Bouchard, D.; Beach, J.; Speiser, D. E.; Mak, T. W.; Ohashi, P. S. *Immunity* **1997**, *7*, 549−557.
(47) Babbitt, B. P.; Allen, P. M.; Matsueda, G.; Haber, E.; Unanue, E. R. *Nature* **1985**, *317*, 359−61.
(48) Kane, K. P.; Mescher, M. F. *J. Immunol.* **1993**, *150*, 4788−4797.
(49) Dustin, M. L.; Miller, J. M.; Ranganath, S.; Vignali, D. A.; Viner, N. J.; Nelson, C. A.; Unanue, E. R. *J. Immunol.* **1996**, *157*, 2014−2021.
(50) Quill, H.; Schwartz, R. H. *J. Immunol.* **1987**, *138*, 3704−3712.
(51) Hoffmann, S.; Hosseini, B. H.; Hecker, M.; Louban, I.; Bulbuc, N.; Garbi, N.; Wabnitz, G. H.; Samstag, Y.; Spatz, J. P.; Hämmerling, G. J. *Immunol. Lett.* **2010**, *136*, 13−20.
(52) Hosseini, B. H.; Louban, I.; Djandji, D.; Wabnitz, G. H.; Deeg, J.; Bulbuc, N.; Samstag, Y.; Gunzer, M.; Spatz, J. P.; Hämmerling, G. J. *Proc. Natl. Acad. Sci. U.S.A.* **2009**, *106*, 17852−7.
(53) Deeg, J. A.; Louban, I.; Aydin, D.; Selhuber-Unkel, C.; Kessler, H.; Spatz, J. P. *Nano Lett.* **2011**, *11*, 1469−76.
(54) Cavalcanti-Adam, E. A.; Aydin, D.; Hirschfeld-Warneken, V. C.; Spatz, J. P. *HFSP J.* **2008**, *2*, 276−285.